Journal of Applied Fluid Mechanics, Vol. 11, No. 6, pp. 1543-1556, 2018.
Available online at www.jafmonline.net, ISSN 1735-3572, EISSN 1735-3645.
DOI: 10.29252/jafm.11.06.28564

Dam-Break Computations by a Dynamical Adaptive Finite Volume Method

Y. Lakhlifi [1†], S. Daoudi [2] and F. Boushaba [1]

[1] *Laboratoire de Mécanique et Modélisation Numérique, ENSAO, Université Mohammed I, Oujda, Maroc.*
[2] *Laboratoire de Mécanique et Energétique, FSO, Université Mohammed I, Oujda, Maroc*

†*Corresponding author: lakhlifiyahya@gmail.com*

(Received November 4, 2017; accepted June 16, 2018)

ABSTRACT

In this paper, a numerical solver is developed for the computation of one and two dimensional dam break problems. The considered equations are the 2D shallow water equations written in conservative form. The algorithm uses a finite volume method which is based on Roe's approximate Riemann solver. It is of second order in space and time, and can be used on complicated geometries with unstructured meshes. The stiffness coming from discontinuity propagation due to the dam is taken into account by the introduction of a dynamical mesh refinement-unrefinement procedure. The results presented on some benchmark dam break situations including wet/dry beds, and comparisons with analytical solutions, show the accuracy of the used methods and the efficiency of the adaptation technique in the simulation of such phenomena.

Keywords: Dam break; Finite volumes; Unstructured meshes; Mesh adaptation; Roe's solver; Dry bed.

1. INTRODUCTION

There are about 45 000 dams in the world, for hydroelectricity, water supply and irrigation, or the regulation of watercourses. Designed to withstand the pressure of water, these dams may still break due to a lack of construction, maintenance or an unexpected event. The phenomenon of dam failure corresponds to a partial or total destruction of a dam. A dam break may be progressive or sudden and results in the formation of a submersion wave resulting in a sudden rise in water level downstream.

Faced with the risk of ruptures of structures such as dams and dykes, scientists are working on the development of hydraulic modeling software. Since the 1980s, many software programs have been developed, and are still used by project managers in the context of dam risk studies (Hervouet, 2000; Delestre *et al*., 2015). For calculations in civil engineering and design, simulations allow to identify and analyze the behaviour of the propagation of the flood wave as well as to give answers on the torrential nature of the flow with the presence of a discontinuous front which propagates towards the downstream, and a rarefaction (depression) wave which propagates upstream. This phenomenon is mathematically described by the set of 2D nonhomogeneous Saint-Venant partial differential equations (shallow water equations), which are derived by the vertical integration of the Navier-Stokes equations along with the assumptions of a hydrostatic pressure and vertically uniform horizontal velocity profile.

Except for some simplified cases, the solutions of the system of Saint-Venant equations can be obtained only by numerical integration. For the correct representation of the dam-beak phenomenon the numerical schemes must also be able to model the sudden variations of the hydraulic parameters without introducing spurious oscillations.

Numerical methods of solution for the shallow water equations has received considerable attention in the past two decades, and many numerical algorithms have been developed (see for instance (Alcrudo and Garcia-Navarro, 1993; Vázquez-Cendón, 1999; Zhou *et al*., 2001; Benkhaldoun *et al*., 2010). Of particular interest has been the prediction of discontinuous solutions to these equations. It is well known that the non linearity combined with the hyperbolic character of the system can produce the appearance of discontinuities even if the initial solution is smooth. For the numerical simulation of dam-beak flows, the most popular schemes are usually associated with the use of Riemann solvers, as they were found to be more consistent in handling the shock-capturing event on most rapidly varied free-surface flows. Bellos *et al*. (1992) adopted a finite volume method for the simulation of the movement on dry

and wet beds of two-dimensional flood waves resulting from the instantaneous break of a dam. Their results were compared and validated with experimental data. Valiani *et al.* (2002) used the finite volume methods based on the Godunov-type scheme to simulate the Malpasset dam-brek event that occurred in southern France in 1959. Rebollo *et al.* (2003) solved the 1D SWE with a flux splitting modeled the 1D drying/wetting fronts with the flux-splitting method. The total-variation diminishing (TVD) Runge-kutta scheme was used by Seaid in (Seaid, 2004) to solve the wet bed sluise gate dam-break and circular dam-break problems, and recently by Luo er al. (2017) who construct two-dimensional shallow water equations, rheological equations and mathematical models of tailings sand flows. Zhou *et al.* (2017) proposed a method based on the three-dimensional k-□ turbulence model, coupled with the volume-of-fluid method, to simulate the dam-break flooding of cascade reservoirs.

In the context of finite element methods, Ortiz (2014) merged the FEM and flux-corrected transport (FCT) techniques for shallow water flows to predict the evolution of coastlines. Seyedashraf and Akhtari (2017) proposed a model which is formulated within the framework of the one-step Taylor–Galerkin scheme in conjunction with the Van Leer's limiter function to the two-dimensional shallow water equations and validate it for the partial, circular, and one dimensional dam-break flow problems. More recently, Zhang *et al.* (2018) used and evaluated the ability of a 3D flood model to predict inundation extent and flood wave travel times in dam-break floods using several testing cases. Their study showed clearly the necessity of 3D modelling technique for dam-break flood simulation when vertical inertia is not negligible.

In the current study, we show the developments of a computational code for the simulation of such a situation. The proposed code, which is under development in our laboratory, is performed in FORTRAN77 language. It is based on the approximate solver technique of Roe (Roe, 1981), which is very appropriate for hyperbolic problem whose solution is often represented by a discontinuous front. Thus, it will be interesting to identify the limit of the proposed code by capturing the shock waves, and to examine the accuracy by simulating torrential flows with the presence of a discontinuity of the velocity profile and the free surface. For this purpose, the finite volume method is used on unstructured meshes in conjunction with a dynamic mesh adaptation method in order to increase the accuracy in regions where the front is steep, such as discontinuities or shock waves. As a consequence, the ability to provide local mesh refinement where it is needed leads to improved accuracy for a given computational cost as compared to methods that use structured meshes. Adaptive mesh refinement (AMR) can facilitate high-resolution simulations of complicated flow with greater accuracy than fixed-grid methods, without making excessive demands on computational resources. AMR typically uses one of two basic strategies: (i) re-meshing, or (ii) local refinement and coarsening. In the remeshing process, the computational grid evolves and/or deforms so as to cluster the grid points in specific regions where high resolution is deemed necessary.

In order to validate the numerical algorithm, we have considered a series of case-studies proposed in the literature such as the drainage due to dam failure on a wet and dry flat bed in a rectangular channel and the 2D partial asymmetric dam break. The objective is to verify the capacity of our code in conjunction with the adaptive mesh refinement to reproduce accurately the characteristics of the 2D propagation of floods following a dam failure.

The paper is organized as follows. In section 2, we present the mathematical equations used to model flows following a dam-break. The formulation of the finite volume method is detailed in section 3. In Section 4 the dynamical mesh adaptation method is presented. Sections 5 and 6 are devoted to numerical results. Finally, section 7 contains some conclusions.

2. 2D SHALLOW WATER EQUATIONS

The model usually used to describe free-surface flows is based on the two-dimensional Saint-Venant equations. These equations predict the spatio-temporal evolution of a free-surface flow in shallow water, characterized by a large horizontal extent in front of the depth. The main significance given by the Saint-Venant equations with respect to the Navier-Stokes equations comes from the hypothesis of a hydrostatic distribution of the pressures in the flow. The terms derived from turbulence, viscosity and wind effects are not taken into account in the study that we consider here.

By integrating the Navier-Stokes equations according along the vertical, the conservative form of the system of equations governing the flow in shallow water can be written as:

$$\begin{cases} \dfrac{\partial h}{\partial t}+\dfrac{\partial (hu)}{\partial x}+\dfrac{\partial (hv)}{\partial y}=0 \\ \dfrac{\partial (hu)}{\partial t}+\dfrac{\partial (hu^2+\frac{1}{2}gh^2)}{\partial x}+\dfrac{\partial (huv)}{\partial y}=-gh\dfrac{\partial Z}{\partial x}-gh\,S_{fx} \\ \dfrac{\partial (hv)}{\partial t}+\dfrac{\partial (huv)}{\partial x}+\dfrac{\partial (hv^2+\frac{1}{2}gh^2)}{\partial y}=-gh\dfrac{\partial Z}{\partial y}-gh\,S_{fy} \end{cases} \quad (1)$$

The variables h, u and v respectively denote the depth of the flow, the longitudinal velocity along the x-direction and the transverse velocity along the y-direction. g is the acceleration of the gravity and $Z(x,y)$ the bed topography function.

The friction losses along the x and y directions are described in terms of the Manning's roughness coefficient n_b:

$$S_{fx}=\frac{n_b^2 u\sqrt{u^2+v^2}}{h^{\frac{4}{3}}} \quad ; \quad S_{fy}=\frac{n_b^2 v\sqrt{u^2+v^2}}{h^{\frac{4}{3}}},$$

In terms of flow variables $W = (h, hu, hv)^t$, the shallow water equations may be written as:

$$\frac{\partial W}{\partial x} + \frac{\partial F(W)}{\partial x} + \frac{\partial G(W)}{\partial y} = S(W) \tag{2}$$

where $S(W)$ is the source term, and $F(W)$ and $G(W)$ are the advection flux functions.

$$W = \begin{pmatrix} h \\ hu \\ hv \end{pmatrix} \quad , \quad F(W) = \begin{pmatrix} hu \\ hu^2 + \frac{1}{2}gh^2 \\ huv \end{pmatrix}$$

$$G(W) = \begin{pmatrix} hv \\ huv \\ hv^2 + \frac{1}{2}gh^2 \end{pmatrix} \quad , \quad S(W) = \begin{pmatrix} 0 \\ -gh\frac{\partial Z}{\partial x} - ghS_{fx} \\ -gh\frac{\partial Z}{\partial y} - ghS_{fy} \end{pmatrix}$$

The system (2) is strictly hyperbolic. The eigenvalues of the Jacobian matrix of the flux function are given by:

$$\begin{cases} \lambda_1 = u.n_x + v.n_y - c \\ \lambda_2 = u.n_x + v.n_y \\ \lambda_3 = u.n_x + v.n_y + c \end{cases}$$

with $c = \sqrt{g\,h}$ the celerity of surface waves.

3. NUMERICAL METHODS

3.1 Finite Volume Discretization

Various methods can be used to discretize the governing equations among which finite volume method is frequently adopted because of its ability to satisfy mass and momentum conservation in the swater equations. This property is a prerequisite for handling reliably discontinuous solutions such as moving hydraulic jumps. The finite volume method is performed here on unstructured triangular meshes. We approach the computational domain $D \subset IR^2$ by $\overline{\Omega}$ subdivided into N_e cells of triangular type such as:

$$\overline{\Omega} = \bigcup_{i=1}^{N_e} T_i$$

We consider the « cell-centered » finite volume formulation, which supposes that the control volumes coincide with the mesh triangles and that the unknowns are the average states on each of these control volumes (see the illustration below).

By integrating the system (2) on a control volume T_i and applying Green's theorem, one obtains:

$$\int_{T_i} \frac{\partial W}{\partial x} dV + \int_{\partial T_i} (F(W)n_x + G(W)n_y)\, d\sigma = \int_{T_i} S(W)\, dV \tag{3}$$

∂T_i being the boundary of the triangle T_i and $n = (n_x, n_y)^T$ the unitary normal to ∂T_i.

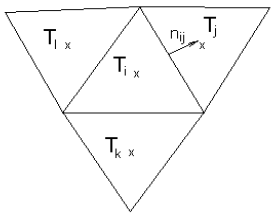

Fig. 1. « Cell-centered » control volume.

A first order time discretization of the system (3) leads to the discrete equations

$$\mathrm{W}_i^{n+1} = \mathrm{W}_i^{n} - \frac{\Delta t}{|\mathrm{T}_i|} \sum_{j \in \mathrm{N}(i)} \int_{\Gamma_{ij}} \mathbf{F}(\mathrm{W}^{n}, \vec{\mathrm{n}})\, \mathrm{d}\sigma + \frac{\Delta t}{|\mathrm{T}_i|} \int_{\mathrm{T}_i} \mathrm{S}(\mathrm{W}^{n})\, \mathrm{dV} \tag{4}$$

where $|T_i|$ is the area of the triangle T_i, $N(i)$ the set of neighboring triangles of T_i by edge, Δt the time step and $\mathbf{F}(W,\vec{n}) = F(W)\,n_x + G(W)\,n_y$ the tensor of physical advection fluxes.

The evaluation of the state W_i^{n+1} on the cell T_i at the time level $n+1$ requires an approximation, on each edge Γ_{ij}, of convective fluxes which can be written in the form:

$$\int_{\Gamma_{ij}} \mathbf{F}(W^n, \vec{n})\, d\sigma = \Phi(W_i^n, W_j^n, \vec{n}_{ij}) \cdot L_{ij}$$

Φ being the numerical flux and L_{ij} the length of the edge Γ_{ij}.

3.2 Roe's Approximate Riemann Solver

The Roe scheme (Roe, 1981) is based on the characteristic decomposition of flow differences by ensuring the conservation of the scheme. It is defined by:

$$\Phi(W_i, W_j, \vec{n}_{ij}) = \frac{1}{2}\left(\mathbf{F}(W_i, \vec{n}_{ij}) + \mathbf{F}(W_j, \vec{n}_{ij})\right) - \frac{1}{2}\left|A(\tilde{W}, \vec{n}_{ij})\right|(W_j - W_i) \tag{5}$$

$A(\tilde{W}, \vec{n}_{ij}) = \tilde{A}(W_i, W_j, \vec{n}_{ij})$ being the Jacobian matrix associated with the convective flux, evaluated on the Roe's average state and satisfies the following conditions (Roe, 1981):

$$\begin{cases} (i)\;\; F(V,\vec{n}) - F(U,\vec{n}) = \tilde{A}(U,V,\vec{n})(V-U); \\ (ii)\;\; \tilde{A} \text{ is diagonalizable with real eigenvalues}; \\ (iii)\; \tilde{A}(U,U,\vec{n}) = \frac{\partial F}{\partial U} n_x + \frac{\partial G}{\partial U} n_y = A(U,\vec{n}) \end{cases}$$

For the system of Saint-Venant equations, $A(\tilde{W}, \vec{n}_{ij})$ is given by:

$$A(\tilde{W},\vec{n}_{ij})=\begin{pmatrix} 0 & n_x & n_y \\ (g\tilde{h}-\tilde{u}^2)n_x-\tilde{u}\tilde{v}n_y & 2\tilde{u}n_x+\tilde{v}n_y & \tilde{u}n_y \\ -\tilde{u}\tilde{v}n_x+(g\tilde{h}-\tilde{v}^2)n_y & \tilde{v}n_x & \tilde{u}n_x+2\tilde{v}n_y \end{pmatrix}$$

$\tilde{u},\tilde{v}\,et\,\tilde{h}$ being the Roe's average states given by:

$$\begin{cases} \tilde{h} = \dfrac{h_i + h_j}{2} \\ \tilde{u} = \dfrac{u_i\sqrt{h_i} + u_j\sqrt{h_j}}{\sqrt{h_i} + \sqrt{h_j}} \\ \tilde{v} = \dfrac{v_i\sqrt{h_i} + v_j\sqrt{h_j}}{\sqrt{h_i} + \sqrt{h_j}} \end{cases}$$

Remembering the decomposition of the Jacobian matrix $|A| = A^+ - A^-$, where A^+ contains all positive and A^- all negative eigenvalues, the Rankine-Hugoniot condition *(i)* allows a simplification of the numerical flux form (5), which can be written in the following ways:

$$\Phi(W_i,W_j,\vec{n}_{ij}) = \mathbf{F}(W_j,\vec{n}_{ij}) - A^+(\tilde{W},\vec{n}_{ij})(W_j - W_i) \qquad (6)$$

$$\Phi(W_i,W_j,\vec{n}_{ij}) = \mathbf{F}(W_i,\vec{n}_{ij}) + A^-(\tilde{W},\vec{n}_{ij})(W_j - W_i) \qquad (7)$$

The great advantage of these formulations, especially in the context of the study of transport of multiple contaminants in shallow water flows, is the low computational effort. The reason for this fact is that at most one eigenvalue of the system has a sign different to all others. Then one of the two terms A^+ or A^- contains at most one eigenvalue, thus becoming very simple to evaluate.

3.3 Treatment of Wet/Dry Regions

In order to handle vacuum states, some modifications on the numerical flux are introduced in the solver as follows:

If h_i and h_j are equal to zero, then set

$$\Phi(W_i, W_j, \vec{n}_{ij}) = 0 \cdot \qquad (8)$$

If $h_i = 0$ and $h_j \neq 0$, then

$$\Phi(W_i, W_j, \vec{n}_{ij}) = \frac{1}{2}\left(\mathbf{F}(W_j,\vec{n}_{ij}) - \left|A(\tilde{W},\vec{n}_{ij})\right| W_j\right) \qquad (9)$$

and a formula similar to Eq. (9) is taken, when $h_i \neq 0$ and $h_j = 0$. These alterations allow calculations to go ahead to final iterations. However, an unphysical stationary jump can appears at the dam location, as the Roe scheme, even modified to handle dry regions, does not ensure the entropy condition. The solution to this problem can be achieved by increasing the numerical dissipation where the numerical viscosity is low (see for instance (Raviart and Godlewski, 1991)). Another approach (Harten and Hyman, 1983), which is considered here, consists in introducing a rarefaction wave wherever the Roe scheme constructs invalid shocks. A correction is required if the left and right sonic eigenvalues of same type have different signs, while representing a rarefaction:

$$\lambda_i = \lambda(W_i) < 0 < \lambda_j = \lambda(W_j)\,.$$

This situation may correspond to a nonphysical shock. To overcome the problem, the eigenvalues are modified. Depending on the simplification chosen, one of the following modifications on the average eigenvalue is required:

$$\lambda^* = \lambda_j\left(\frac{\tilde{\lambda} - \lambda_i}{\lambda_j - \lambda_i}\right) \qquad \text{if Eq. (6) is used,}$$

$$\lambda^* = \lambda_i\left(\frac{\lambda_j - \tilde{\lambda}}{\lambda_j - \lambda_i}\right) \qquad \text{if Eq. (7) is used.}$$

3.4 Extension to Higher Order in Space

In the numerical flux formulations (6) and (7) the states on either side of an edge Γ_{ij} are taken as cell-centered variables W_i and W_j. The resulting scheme is first order in space and is monotonous, but remains poor in precision because of the numerical dissipation. The second-order spatial extension on unstructured meshes can be achieved using the Monotonic Upstream Schemes for Conservation Laws (MUSCL) technique. In this approach, the state W is approached by a system of linear functions by control volume. The left and right states of the edge Γ_{ij} are given by:

$$\begin{cases} W_{ij}^{l} = W_i + \dfrac{1}{2}\vec{\nabla}W_i.\,\overrightarrow{G_iG_j} \\ W_{ij}^{r} = W_j - \dfrac{1}{2}\vec{\nabla}W_j.\overrightarrow{G_iG_j} \end{cases} \qquad (10)$$

where G_i and G_j are respectively the barycentres of the cells T_i and T_j.

To minimize possible nonphysical oscillations that can appear in regions with abrupt changes in the solution, and thus preserve the TVD property of the scheme, we use techniques based on slope limiters. It is preferable to apply simple slope limiters in which the degrees of freedom W_i for a given cell T_i are compared to the average of the approximate solution over T_i and the average of the neighboring cells of the given edge.

In our solver, the following generalized MinMod limiter is introduced (Benkhaldoun *et al.*, 2007):

$$\frac{\partial^{\lim}W_i}{\partial x} = \frac{1}{2}\left[\min_{j\in E(i)}\operatorname{sgn}\left(\frac{\partial W_j}{\partial x}\right) + \max_{j\in E(i)}\operatorname{sgn}\left(\frac{\partial W_j}{\partial x}\right)\right]\min_{j\in E(i)}\left|\frac{\partial W_j}{\partial x}\right|$$

$$\frac{\partial^{\lim}W_i}{\partial y} = \frac{1}{2}\left[\min_{j\in E(i)}\operatorname{sgn}\left(\frac{\partial W_j}{\partial y}\right) + \max_{j\in E(i)}\operatorname{sgn}\left(\frac{\partial W_j}{\partial y}\right)\right]\min_{j\in E(i)}\left|\frac{\partial W_j}{\partial y}\right| \qquad (11)$$

Then, the interpolated left and right values are obtained by replacing in (10) $\vec{\nabla}W_i$ and $\vec{\nabla}W_j$ respectively with $\vec{\nabla}W_i^{\lim}$ and $\vec{\nabla}W_j^{\lim}$. Afterwards, the Roe

numerical flux is calculated using W_{ij}^{l} and W_{ij}^{r}.

It should be pointed out that this slope limiter function is very easy to implement, but it may cause some numerical smoothing of the solution. More sophisticated limiters that are less dissipative such as the one of VanAlbada or Superbee can be used. We refer to (Benkhaldoun *et al*., 2007) for further discussions.

3.5 Time Integration

Since the model is applied to transient flows and flood waves and in order to obtain formally second order accuracy, the time integration is performed by means of a second order accurate and hardly dissipative explicit Runge-Kutta method. As with all explicit time stepping methods, the theoretical maximum stable time step Δt, is specified according to the Courant–Friedrichs–Lewy (CFL) condition

$$\Delta t = Cr \cdot \min_{\Gamma_{ij}} \left(\frac{|T_i| + |T_j|}{2\,|\Gamma_{ij}| \max |\lambda_{ij}^{p}|} \right) \qquad (12)$$

where Γ_{ij} is the edge between the two triangles T_i and T_j, and Cr is a constant to be chosen less than unity. In (12), λ_{ij}^{p} are the eigenvalues of the system (1). In all our simulations, the fixed Courant number $Cr = 0.8$ is used and the time step is varied according to (12), and the gravitational acceleration is fixed to $g = 9.81\ m/s^2$. Furthermore, all the computations are made on a Pentium PC with one processor of 518 MB of RAM and 166 MHz. The code, which is performed in FORTRAN77 language, only takes the default optimization of the machine, that is, it is not parallel code.

3.6 Boundary Conditions

The treatment of boundary conditions in our solver is performed using similar techniques as those described in (Monthe *et al*., 1999).

First, an extra 'ghost' cells are built on the boundary in order to update the boundary conditions. These cells are symmetrical to the adjacent internal ones.

Neumann boundary conditions are then enforced in these boundary cells by setting the required variables to the corresponding values of the adjacent inner cells. In the presence of solid walls limiting the flow field, the velocity is projected into only tangential direction of the wall, in order to represent the absence of a flux through the solid boundary. This simplifies the numerical convection flux expression,

$$\int_{\Gamma_s} \mathbf{F}(W^{n}, \vec{n})\, d\sigma = L_s \cdot \left(0, \frac{g}{2} h_{in}^{2} n_x, \frac{g}{2} h_{in}^{2} n_y \right)^{t}$$

where h_{in} is the water depth at the adjacent inner cell and Γ_s the solid boundary and L_s the length of Γ_s.

4. A DYNAMICAL MESH ADAPTATION METHOD

Dam break phenomena are characterized by the presence of a discontinuous front which propagates downstream the domain and a rarefaction wave which propagates upstream. This stiffness at the front must be taken into account in the numerical scheme. A good numerical scheme must be able to solve this stiffness with a souhaited precision. In addition to the numerical schemes developed, it is clear that the accuracy of the numerical solution is closely related to the fineness and quality of the mesh. The higher the density of the nodes in a mesh, the more accurate the numerical solution, but the more computational time will be. To raise this ambiguity, it is often useful to make a compromise between the numerical precision sought and the complexity of the simulations. One of the ideas developed to counter this difficulty is mesh adaptation. In fact, the real problem in solving a problem with partial differential equations (PDE) is to find a couple "mesh + solution" which makes it possible to obtain, at a lower cost, an approximation of the solution of the PDE to a given precision. This couple is called optimal meshing.

The algorithm we describe here is based on a multi-level hierarchical data structure. It is a dynamical mesh refinement-unrefinement procedure, that is, capable of following the solution of the physical problem. The accuracy is obtained by locally refining the mesh in regions where the structure is interesting (for instance regions with shocks or discontinuities), the efficiency is obtained by successive unrefinements in the zones where the flow is almost regular.

The mesh refinement process consists in dividing all triangles marked for refinement into 4^m sub-triangles by joining the midpoints of their edges, where m represents the number of refinement levels. The method can be repeated in a recursive manner as long as $m < m_{max}$, where m_{max} designates the maximum number of adaptations (see Fig. 2 for an illustration). In our simulations, the refinement is based on a function, called criterion, evaluated on each element of the triangulation. This criterion can be the error of a certain physical variable or also the gradient. The criterion that we consider here is based on the norm of the normalized gradient of the water height.

$$crit\ (T_i) = \frac{\left\| \nabla\,(h(T_i)) \right\|}{\max\limits_{T_j} \left\| \nabla\,(h(T_j)) \right\|} \qquad (13)$$

where $\left\| \nabla(h(T_i)) \right\|$ represents the Euclidean norm of the gradient of the water height in the cell T_i.

From the criterion function, a list L of elements to be refined and those to be unrefined is established. A table *IADIV* of integers is used to define, for each triangle of the list L, the depth m of the required adaptations. For a triangle T_i of the list L, $IADIV(T_i)=m$ means that T_i must be divided in 4^m

sub-triangles. In general, the maximum number, *mmax*, of refinement levels is fixed from the beginning. The coarsest level *l=0* contains a single mesh that converges entirely in the computational domain.

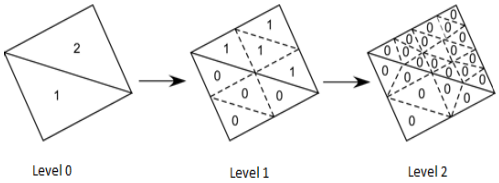

Fig. 2. Example of two refinement levels of a triangular mesh.

5. 1D CONVERGENCE STUDY: MOBILE HYDRAULIC JUMP

As first test case, we consider the propagation of a mobile hydraulic jump along 1D channel of length *50m*. Our objective here is to study the accuracy and convergence of the Roe's scheme in his first and second order versions on different meshes. The hydraulic jump is supposed to move with a constant velocity 2m/s. Initially, the discontinuity is located at $x_0=4.5m$ and the water depth is set to *1m* upstream the discontinuity and *5m* downstream. Thus, the specific discharges have to be *14.13* and *22.12* m^2/s respectively upstream and downstream of the hydraulic jump for the amplitude of the shock to be constant along time. The bottom bed is assumed to be flat and frictionless.

As boundary conditions, the specific discharge *14.13* m^2/s and the water depth *h=1m* are imposed at the upstream limit, which corresponds to a supercritical flow, whereas the flow is subcritical at the downstream limit where only the water depth *h=5m* is imposed.

The computations have been carried out for a period of *20 s*, which is the physical time needed for the hydraulic jump to cover the most of the channel length.

Figure 3 shows the profiles of the water depth at four different physical times t_1*= 5 s,* t_2 *= 10 s,* t_3 *= 15 and* t_4 *= 20 s*, with the mesh size □*x=1m*. A good agreement is obtained for the numerical solution compared to the exact solution, especially near the discontinuity. In addition, the effect of the second-order reconstruction is clearly visible with a local stiffening of the shock.

In order to study the convergence of the mesh convergence, a mesh refining study has been performed with the number of cells N ranging from 50 to 1600 and L_2-error norms of the water depth are evaluated.

In Fig. 4, dependency of *log(error)* versus *log(□x)* is plotted. The order of accuracy of the schemes can be then deduced from the slopes of the lines. The figure shows that the real order of accuracy of the first-order Roe scheme is 0.85 which is lower than 1. This problem is caused because the initial conditions are described by the discontinuous function and the accuracy of the schemes decays near the discontinuities. The order of accuracy is increased to 1.2 when the linear reconstruction is used.

6. DAM BREAK COMPUTATIONS

Flows due to floods produced by a dam failure, segments of dykes, or other structures are torrential in nature with the presence of a discontinuous front that propagates downstream and a rarefaction which propagates upstream. The characteristics of such flows such as velocity, water level and flood arrival time must be determined in advance for flood management and a reduction in their impact on the environment and economic infrastructure.

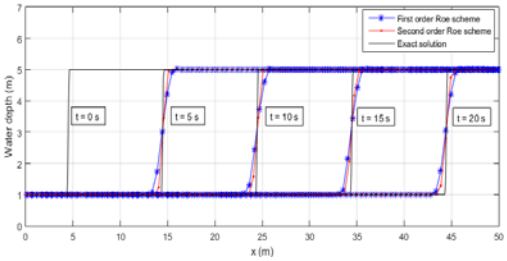

Fig. 3. Propagation of a mobile hydraulic jump.

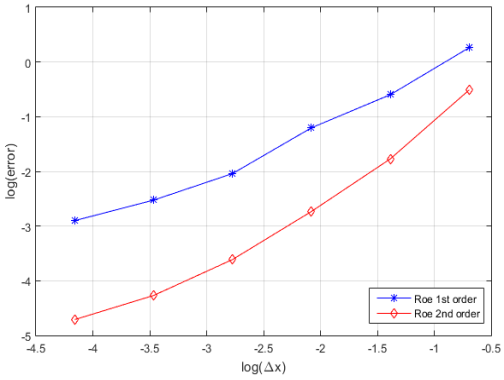

Fig. 4. L_2-error of first and second order Roe schemes.

In order to validate the proposed numerical schemes for problems related to dam failure, we present some model test cases proposed in the literature (see, among others (Fennema and Chaudhry, 1990; Brufau and Garcıa-Navarro, 2003)). The two first tests are 1D and consist of flow due to dam break on a flat, non-friction wet or dry bottom in a rectangular channel of constant width. The third test is a 2D flow due to partial dam break on a wet, flat, bottom, with friction, in a rectangular channel of variable width.

6.1 Ideal Dam-Break on a Wet Domain

6.1.1 Problem description

A one-dimensional problem which has a known analytical solution given by Stoker (Stoker 1957) is used to assess the accuracy of the numerical algorithm. We consider a torrential flow in a rectangular channel with flat bottom and without friction. In this case, the problem is purely hyperbolic. A dam is placed in the middle of a channel of length *L=12 m*, and is abruptly removed at *t = 0 s* to cause a shock wave which propagates downstream of the channel.

The Fig. 5 shows the initial condition of the

problem. Upstream of the dam, the water is retained at a depth $h_1 = 5m$, the downstream part represents a thin layer of water of thickness $h_2 = 1m$ at rest $(u = 0\ m/s)$.

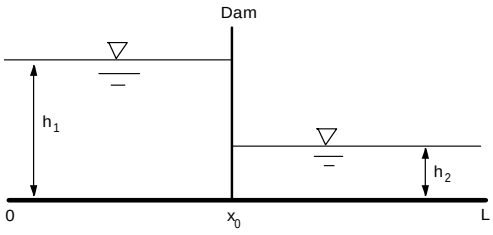

Fig. 5. Initial condition for the 1D dam-break problem.

This model corresponds to an homogeneous Riemann problem. Works made by Hsu and Yeh (Hsu and Yeh, 2002) showed that the parameter $\beta = h_2/h_1$ is a good control parameter for studying the numerical stability of the flow. These works, using a projection numerical scheme, allowed to obtain a critical value β_c of this parameter ($\beta_c = 0.138$). They showed that if $\beta > \beta_c$ the flow is subcritical throughout the basin. For $\beta < \beta_c$, the flow is supercritical downstream and subcritical upstream of the rupture position. They also showed that for $\beta << \beta_c$ the flow regime at the upstream becomes highly supercritical and it becomes difficult to numerically capture such a shock wave because the shape and the celerity of the front of the numerical shock are significantly removed from the analytical solution.

For the test case considered here and in order to test the stability of our numerical scheme we performed the numerical simulation of the flow for the value β=0.2. The water height and the speed obtained by our model will be compared with the analytical solution which is obtained thanks to the characteristics method as (Stoker 1957):

$$h(x,t) = \begin{cases} h_1 \\ \dfrac{1}{9g}\left(2\sqrt{gh_1} - \dfrac{x-x_0}{t}\right)^2 \\ h_m \\ h_2 \end{cases}$$

$$u(x,t) = \begin{cases} 0 & if\ x \le x_1 \\ \dfrac{2}{3}\left(\sqrt{gh_1} + \dfrac{x-x_0}{t}\right) & if\ x_1 \le x \le x_2 \\ u_m & if\ x_2 \le x \le x_3 \\ 0 & if\ x_3 \le x \end{cases} \quad (14)$$

Where

$$x_1 = x_0 - t\sqrt{gh_1},\quad x_2 = x_0 + \left(u_m - \sqrt{gh_m}\right),$$

$$x_3 = x_0 + s.t = x_0 + t \cdot \sqrt{\frac{gh_m}{2}\left(\frac{h_m}{h_2} + 1\right)}$$

h_m, u_m and s denote respectively the water depth, the speed and the speed of propagation of the shock. They are given by:

$$h_m = \frac{1}{2}\left(\sqrt{1 + \frac{8s^2}{gh_2}} - 1\right)h_2$$

$$u_m = s - \frac{gh_2}{4s}\left(\sqrt{1 + \frac{8s^2}{gh_2}} + 1\right) \quad (15)$$

$$u_m + 2\sqrt{gh_m} - 2\sqrt{gh_1} = 0$$

The first two equations in (15) describe the Rankine-Hugoniot relations at the front of the discontinuity shock. The last equation represents the invariable conservation of Riemann. The resolution of this nonlinear system, by a Newton-Raphson method, gives the following values of h_m, u_m and s:

$$h_m = 2.534\ m, \qquad u_m = 4.03\ m/s, \quad \text{and}$$

$$s^2 = \frac{gh_m}{2}\left(\frac{h_m}{h_2} + 1\right) = 7.19$$

6.1.2 Results and Discussion

We compare the results on three types of meshes, a coarse mesh consisting of 2363 triangles and 1276 nodes, a fine mesh consisting of 37808 triangles and 19279 nodes, and a dynamical adaptive mesh that follows stiff fronts of the flow. The Fig. 6 shows the coarse and fine meshes respectively at the initial state.

Figures 7, 8 and 9 shows a 3D view of the water depth at three physical times t = 0.2, 0.4 and 0.6 s, as well as the associated dynamical adaptive meshes. The mesh adaptation at the rarefaction and shock wave zones is clearly illustrated. Moreover, this stiffness at the shock front is captured in a very accurate manner without the occurrence of oscillations, which shows that the refinement-unrefinement process is able to follow dynamically these stiff structures.

In order to compare the accuracy of the solver on the three types of meshes, we have performed 1D cross-sections on the water depth and velocity in x-direction along the y-axis (y = 1m). These sections are shown in the Fig. 10 at the time t = 0.4 s. An excellent agreement is obtained between the numerical and analytical results. These figures clearly show the capacity of the numerical schemes to capture shocks at the discontinuity level. Using adaptive meshes, a high resolution is obtained automatically in regions where the gradients of the water depth are steep. It should also be noted that the overall flow regime for this example, using the Roe scheme on adaptive mesh, is preserved without the apparition of oscillations. Let's mention also that, some numerical schemes, reported by Jha *et al.* (Jha *et al.*, 1995) have shown a pronounced vertical drop in the water depth profile at the dam location, which is nonphysical. In the present simulations, such vertical drop is almost invisible.

In order to quantify these results, the errors in norm L_2 of the water depth and u-velocity are presented in Table 1, calculating:

$$\left\| h_{Num} - h_{Exact} \right\|_2 = \left(\int_0^L \left(h_{Num} - h_{Exact} \right)^2 dx \right)^{1/2}$$

$$\left\| u_{Num} - u_{Exact} \right\|_2 = \left(\int_0^L \left(u_{Num} - u_{Exact} \right)^2 dx \right)^{1/2}$$

Table 1 Errors on the water depth and velocity u, and CPU time on the three meshes at time t = 0.4 s.

	Coarse mesh	Fine mesh	Adaptive mesh
Nodes	1276	19279	7907
Triangles	2363	37808	15485
Errors on h	$2.27\ 10^{-2}$	$5.54\ 10^{-3}$	$2.23\ 10^{-3}$
Errors on u	$8.49\ 10^{-2}$	$9.38\ 10^{-3}$	$5.86\ 10^{-3}$
CPU time (s)	1.34	95.4	80.5

It is clear from the table 1 that the errors on *h* and *u* obtained on the adaptive meshes are much lower than those on the coarse and fine meshes. In Table 1, we also evaluated the CPU time obtained on each mesh to perform simulations up to the physical time t = 0.4 s. We can remark here also that the CPU time obtained by calculating on dynamical adaptive meshes is lower than that on fine meshes, while keeping a more accurate solution. All these results show that the use of dynamical meshes is much efficient especially in the simulation of long flow problems such as the study of hydrodynamics or the transport of contaminants in rivers or oceans.

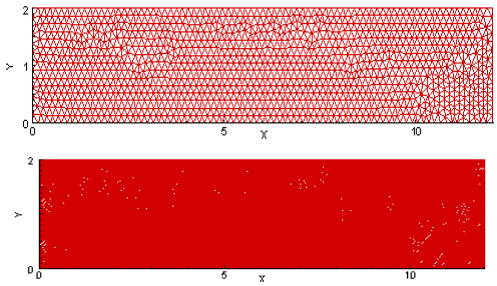

Fig. 6. Coarse mesh (top) and fine mesh (bottom).

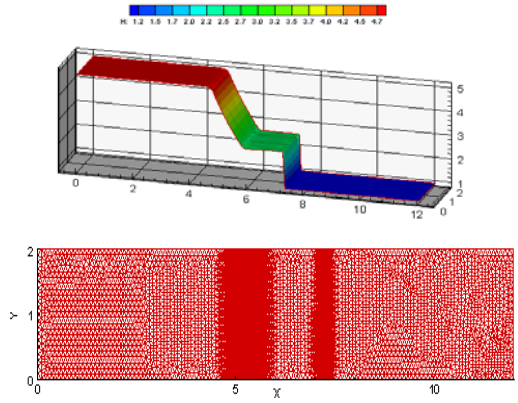

Fig. 7. Water depth and adaptive mesh at physical time t=0.2 s.

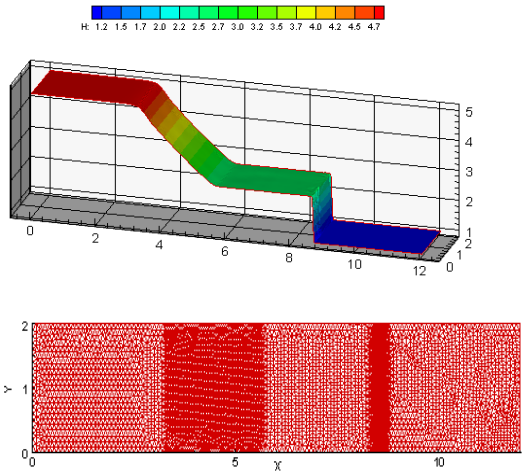

Fig. 8. Water depth and adaptive mesh at physical time t=0.4 s.

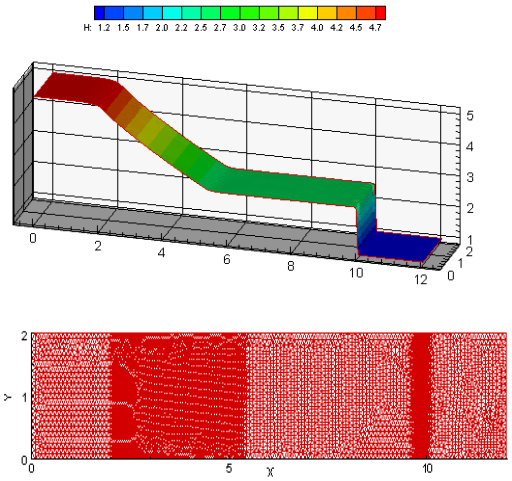

Fig. 9. Water depth and adaptive mesh at physical time t=0.6 s.

6.2 Ideal Dam-Break on a Dry Domain

The initial upstream and downstream water levels for this test are *5m* and *0m* respectively and the simulation time is *0.2s*. It is expected that propagation wave moves downwards while a rarefaction wave goes back in the reservoir. The analytical calculation of the dam-break wave propagation on smooth dry bed has been performed for the first time by Ritter. It is given by

$$h(x,t) = \begin{cases} h_1 \\ \dfrac{1}{9g}\left(2\sqrt{gh_1} - \dfrac{x - x_0}{t} \right)^2 \\ 0 \end{cases}$$

and

$$u(x,t) = \begin{cases} 0 & if\ x \le x_1 \\ \dfrac{2}{3}\left(\sqrt{gh_1} + \dfrac{x - x_0}{t} \right) & if\ x_1 \le x \le x_2 \\ 0 & if\ x_2 \le x \end{cases} \quad (16)$$

where $x_1 = x_0 - t\sqrt{gh_1}$, $x_2 = x_0 + 2t\sqrt{gh_1}$

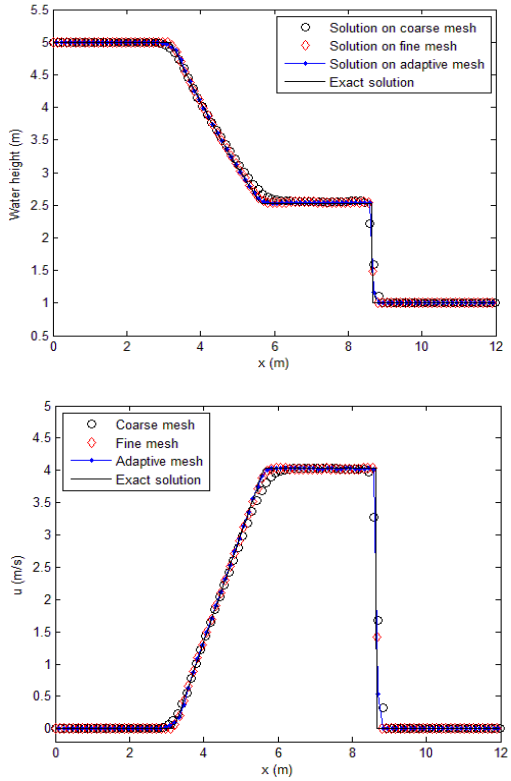

Fig. 10. 1D cross-section on the water depth (top) and velocity u (bottom) along the y-axis (y=1m) at time t = 0.4 s.

This solution will show if the scheme is able to locate and treat correctly the wet/dry transition. It also emphasizes whether the scheme preserves the positivity of the water height, as this property is usually violated near the wetting front.

Figures 11 show the simulated and theoretical water depth and u-velocity profiles at time $t = 0.2\ s$ after the dam-break. The results show an excellent agreement with analytical solutions. Both shock wave and rarefaction wave are predicted without any numerical oscillation. The accuracy of the solution by the adaptive procedure is clearly seen on the velocity profile. This is also clearly visible in the contour plots and the dynamical adaptive mesh of Figs. 12, where the shock wave is captured with high resolution.

6.3 Partial Dam Break

6.3.1 Description of the Problem

The test cases presented previously are one-dimensional. In reality, torrential flows due to dam break and dike segments are often two-dimensional. Our objective here is to verify the capacity of our model to reproduce the two-dimensional propagation of floods in the presence of a discontinuous front of the water height and the velocity on a wet flat bottom.

One considers the torrential flow due to partial and asymmetric dam break. This problem, which was proposed by Fennema and Chaudhry (Fennema and Chaudhry, 1990) is widely used by many researchers to validate their dam break models. The particular interest is that its solution is characterized by: i) a shock wave which propagates downstream by abruptly increasing the water height and is modified by a reflection wave (when it collides with the wall), and ii) a rarefaction (depression) wave, which moves upstream by decreasing the water height, often described as a rarefaction shock.

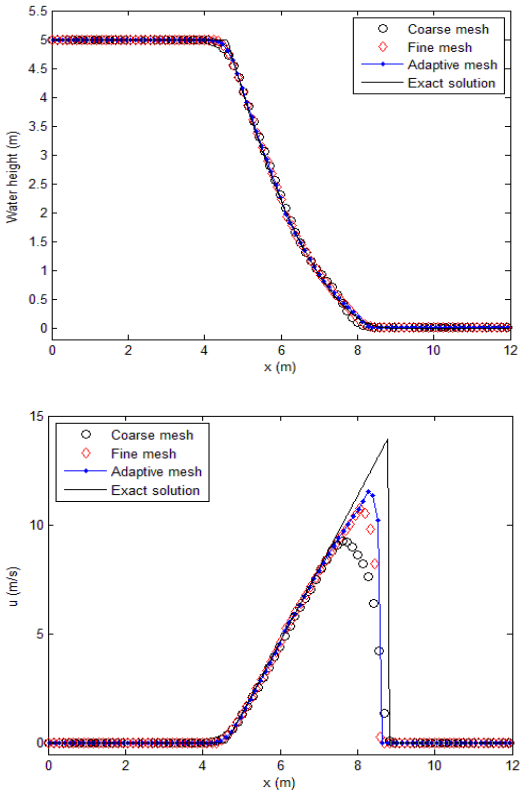

Fig. 11. 1D cross-section on h and u along the y-axis (y=1m) at time t = 0.2 s.

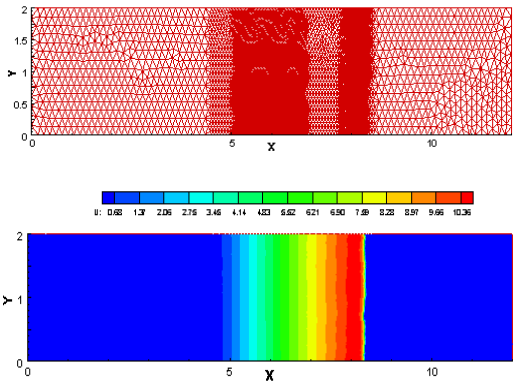

Fig. 12. Adaptive mesh (top) and contour plot of u (bottom) at time t = 0.2 s.

The study area is a $200\,m$ wide basin, $200m$ long and has flat bottom. The water is retained in the left part of the basin. It is assumed that at t = 0 s, suddenly the reservoir of the dam is in partial rupture and is non-symmetrical along a length of $75\,m$. The thickness of the dam is $10\,m$ on the flow direction. Figure 13 gives a geometric

description of this problem. It should be noted that there is no analytical solution to this two-dimensional problem, but the results can be compared with those of other numerical schemes such as (Fujihara and Borthwick (2000), Wang *et al*. (2000), Liang *et al*. (2007)).

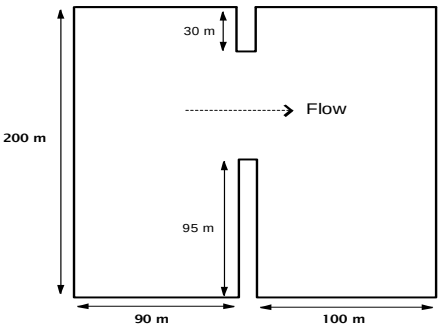

Fig. 13. Partial dam break: Geometry of the basin.

A ratio of $h_2/h_1=0.5$ is initially fixed with $h_1=10m$ the water height in the reservoir and $h_2=5m$ the water height downstream of the dam. The water in the basin is assumed to be at rest in the initial state. In this simulation, the wall and bottom friction are taken into account by calibrating the Manning number to $0.03\ s/m^{1/3}$.

6.3.2 Results

The domain studied was initially discretized with 1814 nodes and 3416 triangles whose sizes are regularly fixed at *5m*, the time step Δt is chosen such that the stability condition (12) is satisfied.

At the instant of dam breaking, water is released through the 75m-wide sluice-gate. A forward bore wave is formed at downstream of the channel; while negative depression wave is generated at the upstream.

Figures 14 and 15 show the results at physical times 4 s and 8 s. In these figures, we display the three-dimensional free surfaces, the water height isolines, the dynamical adaptive meshes and the velocity fields. We can observe that the right-moving flow propagates to the downstream up and down, rarefaction wave propagates to the upstream and two asymmetric weak vortices are developed on both sides on the breach.

It is evident that with the use of adaptive meshes, a high resolution is automatically obtained in those regions where the gradients of the water depth are steep, such as the moving fronts. Apparently, the overall flow for this example is preserved with no excessive numerical diffusion in the results by finite-volume method using the three-level adaptive mesh. Our results seem to be very similar to those presented by the existing and previously mentioned studies.

We notice also a very slight shrinking of the free surface at the wavefront. This increase is also observed in the results presented by Fennema and Chaudhry, without artificial viscosity (see Fig. 4 in (Fennema and Chaudhry, 1990).

In order to show the contribution of the adaptation process, the same simulations were carried out on two types of meshes: the coarse mesh with 1814 nodes and 3416 triangles, and a fine mesh with 27749 nodes and 54656 triangles. A reference solution is also used to quantify the numerical results obtained on the three different meshes.

In Tables 2 and 3, the accuracy analysis results are summarized. In these tables, we list the mesh statistics, the L_2-error norm of the water depth h and u-velocity and the CPU time obtained on each mesh to perform simulations up to the physical times 4 s and 8 s. In Figs. 16 and 17, we present the cross-sections of h and u along y-axis y=100m and y=125m at time t = 4 s.

First, from these figures it can be seen that the numerical prediction obtained using the second order MinMod limiter is significantly less diffusive (and hence more accurate) than that using the first order Roe scheme. Comparisons between errors of the solutions obtained on the coarse mesh using first and second order Roe scheme (see tables 2 and 3), show that the diffusive effect increases progressively with simulation times which can have serious negative impact on the accurate prediction of fronts when the simulation time is long.

Figures 16 and 17 show also clearly that Roe scheme on adaptive meshes overcome the Roe scheme on fixed coarse and fine meshes, which is also demonstrated on the residual of h and u in tables 2 and 3. The residual on h over the adaptive mesh is smaller than the one on the fixed fine mesh and is reduced more than 80% from the residual on the fixed coarse mesh. An examination of the CPU times in tables 2 and 3 reveals that, Roe scheme on fixed fine mesh requires more computational work than its adaptive counterpart while the results are more accurate. A balance between efficiency and accuracy in Roe schemes benefits the second order adaptive Roe scheme, since the additional cost required for the adaptation procedure is minimal while the results obtained by adaptive Roe schemes are more accurate than those obtained by Roe schemes on fixed meshes.

7. CONCLUSION

In this study, we developed a computation code for the prediction of risks due to dam-break phenomena. The numerical model solves the coupled non-linear shallow water equations by means of a second-order finite volume Roe's method in conjunction with a dynamical mesh adaptation process. Two academic test cases have been simulated: a 1D ideal dam-break flow and a 2D partial dam break flow. For both test cases, numerical simulations have conducted on coarse meshes, fine meshes and adaptive meshes, and the solutions were compared to the analytical solutions or a reference solution.

The results have shown that the use of the first order Roe scheme leads to more diffusive numerical solution, which can have serious negative impact on the accurate prediction of fronts when the simulation time is long. The introduction of the second order with MUSCL technique reduces this diffusion in the solution.

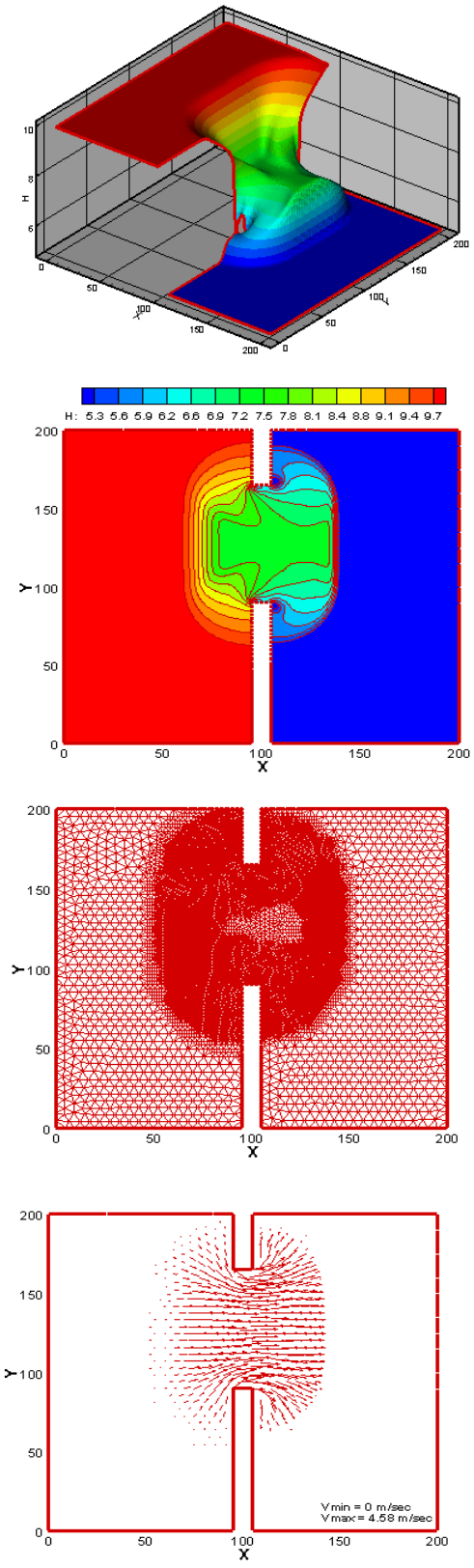

Fig. 14. 3D free surface, contour of h, adaptive mesh and velocity field at the simulation time t=4 s.

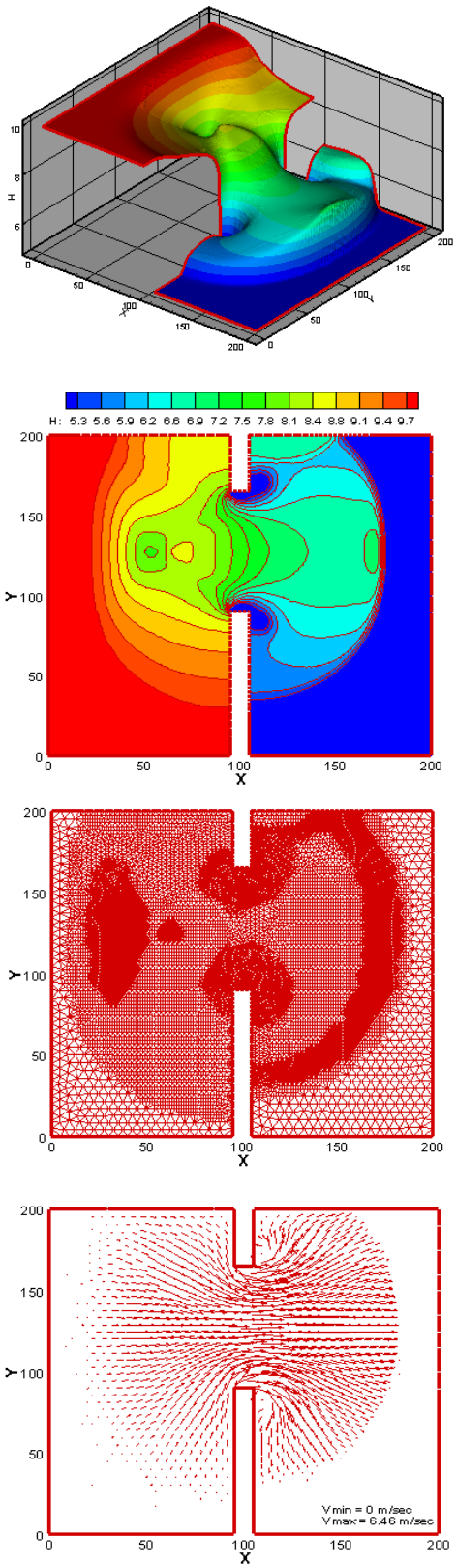

Fig. 15. 3D free surface, contour of h, adaptive.mesh and velocity field at the simulation time t=8 s.

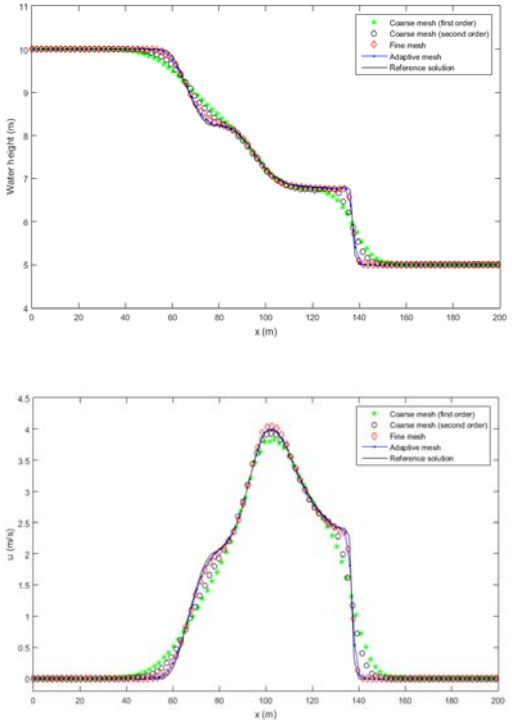

Fig. 16. 1D cross-section on the water depth (top) and u-velocity (bottom) along the y-axis (y=100m) at time t = 4 s.

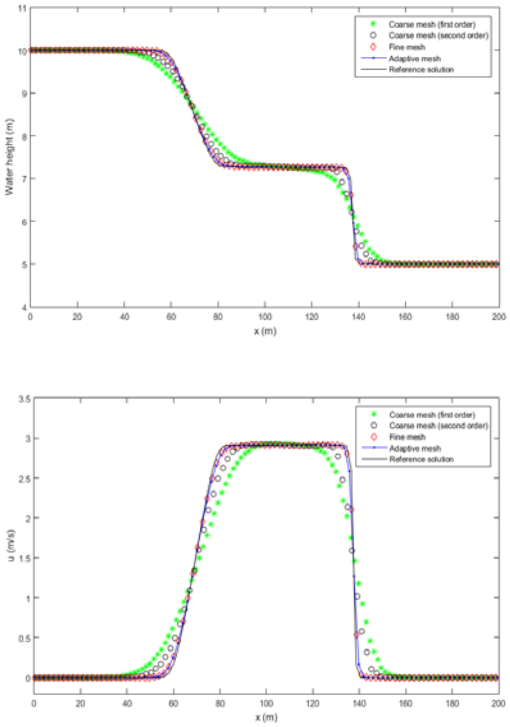

Fig. 17. 1D cross-section on the water depth (top) and u-velocity (bottom) along the y-axis (y=125m) at time t = 4 s.

Table 2 Errors on the water depth and u-velocity, and CPU time on the three meshes at time t = 4 s.

	Coarse mesh 1st order	Coarse mesh 2nd order	Fine mesh	Adaptive mesh
Nodes	1814	1814	27749	9509
Triangles	3416	3416	54656	18689
Errors on h	$6.37\ 10^{-2}$	$4.84\ 10^{-2}$	$8.26\ 10^{-3}$	$7.90\ 10^{-3}$
Errors on u	$7.45\ 10^{-2}$	$5.58\ 10^{-2}$	$9.15\ 10^{-3}$	$8.18\ 10^{-3}$
CPU time (s)	5.3	8.9	723.5	156.5

Table 3 Errors on the water depth and u-velocity, and CPU time on the three meshes at time t = 8 s.

	Coarse mesh 1st order	Coarse mesh 2nd order	Fine mesh	Adaptive mesh
Nodes	1814	1814	27749	10977
Triangles	3416	3416	54656	21610
Errors on h	$8.62\ 10^{-2}$	$5.94\ 10^{-2}$	$9.23\ 10^{-3}$	$8.58\ 10^{-3}$
Errors on u	$9.32\ 10^{-2}$	$6.67\ 10^{-2}$	$9.85\ 10^{-3}$	$8.72\ 10^{-3}$
CPU time (s)	10.5	19.2	1533.4	512.8

Furthermore, it was demonstrated that the use of the mesh adaptation method to simulate these problems has considerably increased the accuracy and precision of the results with a very significant simulation time saving.

The overall results on different meshes and the comparisons with analytical or reference solutions have demonstrated the robustness of our model and shown a good agreement with those in the literature. In particular, the algorithm can handle with accuracy the stiff fronts such as shock waves in the simulation of these phenomena.

Finally, let's mention that the algorithm exhibits many desirable properties in the numerical solution of shallow water flows and it is attractive for general purpose flow modeling for several reasons including:

- Accurate prediction of the free surface with correct conservation properties.

- Good convergence behaviors with respect to computational refinement and high efficiency compared with computations on fixed meshes.

- Implementation on triangular grids that can be easily generated for the hydrodynamic study in complex geometries.

REFERENCES

Alcrudo, F. and P. Garcia-Navarro (1993). A high-resolution Godunov-type scheme in finite volumes for the 2D shallow-water equations. *International Journal for Numerical Methods in Fluids* 16 (6), 489-505.

Bellos, C. V., V. Soulis and J. G. Sakkas (1992). Experimental investigation of two-dimensional dam-break induced flows, *Journal of Hydraulic Research* 30 (1), 47-63.

Benkhaldoun, F., I. Elmahi and M. Seaı (2007). Well-balanced finite volume schemes for pollutant transport by shallow water equations on unstructured meshes, *Journal of computational physics* 226 (1), 180-203.

Benkhaldoun, F., I. Elmahi and M. Seaïd (2010). A new finite volume method for flux-gradient and source-term balancing in shallow water equations, *Computer Methods in Applied Mechanics and Engineering* 199 (49), 3324-3335.

Brufau, P. and P. Garcıa-Navarro (2003). Unsteady free surface flow simulation over complex topography with a multidimensional upwind technique, *Journal of Computational Physics* 186 (2), 503-526.

Delestre, O., F. Darboux, F. James, C. Lucas, C. Laguerre and S. Cordier (2015). FullSWOF: A free software package for the simulation of shallow water flows, *Research report* [hal-00932234].

Fennema, R. J. and M. H. Chaudhry (1990). Explicit methods for 2-D transient free surface flows, *Journal of Hydraulic Engineering* 116 (8), 1013-1034.

Fujihara, M. and G. L. Borthwick (2000). Godunov-type solution of curvilinear shallow-water equations, *Journal of Hydraulic Engineering, ASCE* 126(11), 827–836.

Godlewski, E. and P. A. Raviart (1991). Hyperbolic systems of conservation laws, *Ellipses, Paris*.

Harten, A. and J. M. Hyman (1983). Self adjusting grid methods for one-dimensional hyperbolic conservation laws, *Journal of computational Physics* 50 (2), 235-269.

Hervouet, J. M. (2000). TELEMAC modelling system: an overview, *Hydrological Processes* 14 (13), 2209-2210.

Hsu, C. T. and K. C. Yeh (2002). Iterative explicit simulation of 1D surges and dam-break flows, *International journal for numerical methods in fluids* 38 (7), 647-675.

Jha, A. K., J. Akiyama and M. Ura (1995). First-and second-order flux difference splitting schemes for dam-break problem, *Journal of Hydraulic Engineering* 121 (12), 877-884.

Liang, D., B. Lin and R. A. Falconer (2007), Simulation of rapidly varying flow using an efficient TVD-MacCormack scheme, *International Journal for Numerical Methods in Fluids* 53, 811–826.

Luo, C., K. Xu, and Y. Zhao (2017), TVD discretization method for shallow water equations: Numerical simulations of tailing dam break, *International Journal of Modeling, Simulation and Scientific Computing* 8 (3), 22 pages.

Monthe, L. A., F. Benkhaldoun and I. Elmahi (1999), Positivity preserving finite volume Roe schemes for transport-diffusion equations. *Computer Methods in Applied Mechanics and Engineerings* 178*, 215–232.*

Ortiz, P. (2014), Shallow water flows over flooding areas by a flux-corrected finite element method, *Journal of Hydraulic Research* 52 (2), 241–252.

Rebollo, T. C., Nieto, E. D. F. and Marmol, M. G. (2003). A flux-splitting solver for shallow water equations with source terms, *International journal for numerical methods in fluids* 42 (1), 23-55.

Roe, P. L. (1981). Approximate Riemann solvers, parameter vectors, and difference schemes, *Journal of computational physics* 43 (2), 357-372.

Seaïd, M. (2004). Non-oscillatory relaxation methods for the shallow-water equations in one and two space dimensions, *International Journal for Numerical Methods in Fluids* 46 (5), 457-484.

Seyedashraf, O. and A. A. Akhtari (2017), Two‐dimensional numerical modeling of dam‐break flow using a new TVD finite‐element scheme, *Journal of the Brazilian Society of Mechanical Sciences and Engineering* 39 (11), 4393-4401.

Stoker, J. J. (1957), Water Waves, *The Mathematical Theory with Applications*, Interscience, London.

Valiani, A., V. Caleffi, and A. Zanni (2002). Case study: Malpasset dam-break simulation using a two-dimensional finite volume method, *Journal of Hydraulic Engineering* 128 (5), 460-472.

Vázquez-Cendón, M. E. (1999).Improved treatment of source terms in upwind schemes for the shallow water equations in channels with irregular geometry, *Journal of Computational Physics* 148 (2), 497-526.

Wang, J. S., H. G. Ni and Y. S. He (2000). Finite difference TVD scheme for computation of dam break problems, *Journal of Hydraulic*

Engineering, ASCE 126(4), 253–262.

Zhang, T., L. Peng, P. Feng (2018), Evaluation of a 3D unstructured-mesh finite element model for dam-break floods, *Computers and Fluids* 160*, 64-77*.

Zhou, J. G., D. M. Causon, C. G. Mingham and D. M. Ingram (2001). The surface gradient method for the treatment of source terms in the shallow-water equations, *Journal of Computational physics* 168 (1), 1-25.

Zhou, Z., X. Wang, W. Chen, S. Deng and M. Liu (2017), Numerical simulation of dam-break flooding of cascade reservoirs, *Transactions of Tianjin University* 23 (6), 570-581.